

---

---

# Site-Specific and Residualizing Linker for $^{18}\text{F}$ Labeling with Enhanced Renal Clearance: Application to an Anti-HER2 Single-Domain Antibody Fragment

Zhengyuan Zhou, Rebecca Meshaw, Michael R. Zalutsky, and Ganesan Vaidyanathan

Department of Radiology, Duke University Medical Center, Durham, North Carolina

---

Single-domain antibody fragments (sdAbs) are promising vectors for immuno-PET; however, better methods for labeling sdAbs with  $^{18}\text{F}$  are needed. Herein, we evaluate a site-specific strategy using an  $^{18}\text{F}$  residualizing motif and the anti-epidermal growth factor receptor 2 (HER2) sdAb 5F7 bearing an engineered C-terminal GGC tail (5F7GGC).

**Methods:** 5F7GGC was site-specifically attached with a tetrazine-bearing agent via thiol-maleimide reaction. The resultant conjugate was labeled with  $^{18}\text{F}$  by inverse electron demand Diels–Alder cycloaddition with a *trans*-cyclooctene attached to 6- $^{18}\text{F}$ -fluoronicotinoyl moiety via a renal brush border enzyme-cleavable linker and a PEG<sub>4</sub> chain ( $^{18}\text{F}$ -5F7GGC). For comparisons, 5F7 sdAb was labeled using the prototypical residualizing agent, *N*-succinimidyl 3-(guanidinomethyl)-5- $^{125}\text{I}$ -iodobenzoate (*iso*- $^{125}\text{I}$ -SGMIB). The 2 labeled sdAbs were compared in paired-label studies performed in the HER2-expressing BT474M1 breast carcinoma cell line and athymic mice bearing BT474M1 subcutaneous xenografts. Small-animal PET/CT imaging after administration of  $^{18}\text{F}$ -5F7GGC in the above mouse model was also performed. **Results:**  $^{18}\text{F}$ -5F7GGC was synthesized in an overall radiochemical yield of  $8.9\% \pm 3.2\%$  with retention of HER2 binding affinity and immunoreactivity. The total cell-associated and intracellular activity for  $^{18}\text{F}$ -5F7GGC was similar to that for coincubated *iso*- $^{125}\text{I}$ -SGMIB-5F7. Likewise, the uptake of  $^{18}\text{F}$ -5F7GGC in BT474M1 xenografts in mice was similar to that for *iso*- $^{125}\text{I}$ -SGMIB-5F7; however,  $^{18}\text{F}$ -5F7GGC exhibited significantly more rapid clearance from the kidney. Small-animal PET/CT imaging confirmed high uptake and retention in the tumor with very little background activity at 3 h except in the bladder. **Conclusion:** This site-specific and residualizing  $^{18}\text{F}$ -labeling strategy could facilitate clinical translation of 5F7 anti-HER2 sdAb as well as other sdAbs for immuno-PET.

**Key Words:** single-domain antibody fragment; site-specific labeling; immuno-PET; click chemistry; HER2

**J Nucl Med 2021; 62:1624–1630**  
DOI: 10.2967/jnumed.120.261446

---

**S**maller protein scaffolds exemplified by 6-kDa Affibody molecules (Affibody AB) and 12- to 15-kDa single-domain antibody fragments (sdAbs) have emerged as promising platforms for theranostics because they possess properties intermediate between those of monoclonal antibodies and peptides. A recent review (1) has summarized efforts with these delivery vehicles to image and treat

cancers overexpressing epidermal growth factor receptor 2 (HER2), an internalizing receptor that is overexpressed in breast, ovarian, gastric, and other cancers (2). Because only about 20%–25% of breast cancers are HER2-positive and metastatic disease frequently exhibits heterogeneities in HER2 expression, assessment of HER2 status is imperative before embarking on HER2-targeted therapies (3).

Combining an anti-HER2 sdAb with a radiolabeling strategy tuned to the properties of small proteins could provide a promising immuno-PET approach for global and repeatable evaluation of HER2 status. Given the high and prolonged uptake of radiometal-labeled sdAbs in kidneys (1,4),  $^{18}\text{F}$  is a promising radionuclide for sdAb-based immuno-PET. Moreover,  $^{18}\text{F}$  has a half-life compatible with the rapid clearance of sdAbs, positron emission characteristics that are ideal for imaging, and a readily available supply chain. Although several  $^{18}\text{F}$  protein labeling methods have been developed (5), *N*-succinimidyl 4- $^{18}\text{F}$ -fluorobenzoate ( $^{18}\text{F}$ -SFB) (6) remains the most widely used reagent for this purpose. Both our group (7) and others (8) have labeled sdAbs with  $^{18}\text{F}$ -SFB; however, the nonresidualizing capacity of  $^{18}\text{F}$ -SFB compromised tumor retention of  $^{18}\text{F}$  after receptor-mediated internalization.

Studies with  $^{131}\text{I}$ - and  $^{211}\text{At}$ -labeled HER2-targeted sdAbs have demonstrated that very effective trapping of radioactivity in tumor can be achieved using charged prosthetic groups (9–11). In recent years, we have developed conceptually similar prosthetic agents for labeling sdAbs with  $^{18}\text{F}$  (7,12,13). Two tactics that we investigated were the very fast tetrazine (Tz)-*trans*-cyclooctene (TCO) inverse electron demand Diels–Alder cycloaddition reaction (IED-DAR) and exploiting a renal brush border enzyme (RBBE)-cleavable linker to reduce kidney activity (12,14). In these studies,  $^{18}\text{F}$  was introduced on the Tz-bearing moiety. Although kidney activity could be reduced considerably, activity in hepatobiliary organs was elevated, presumably because of the high lipophilicity of Tz-bearing radiocatabolites (15,16).

Herein we describe a new linker for  $^{18}\text{F}$  labeling of the HER2-targeted sdAb 5F7 that also could be applied in principle to site-specific labeling of other proteins with engineered cysteine residues via thiol-maleimide conjugation (17). Precise control of the  $^{18}\text{F}$ -labeling site on the C terminus of an sdAb can avoid chemical modification of amino acids involved in receptor/antigen recognition and provide a uniform product more amenable to clinical translation (18). Other design features of this linker include the use of the 6- $^{18}\text{F}$ -fluoronicotinoyl group for residualization (13), and a GlyLys RBBE-cleavable linker strategically positioned within its structure (Fig. 1) to create rapid, high contrast between tumor and both kidneys and hepatobiliary organs.

---

Received Dec. 6, 2020; revision accepted Feb. 1, 2021.  
For correspondence or reprints, contact Ganesan Vaidyanathan (ganesan.v@duke.edu).  
Published online February 26, 2021.  
COPYRIGHT © 2021 by the Society of Nuclear Medicine and Molecular Imaging

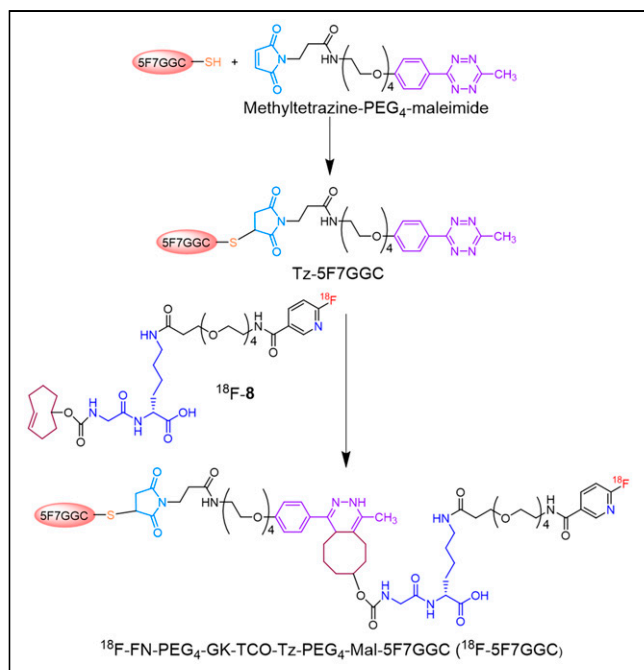


**FIGURE 1.** Scheme for synthesis of  $^{18}\text{F}$ -FN-PEG<sub>4</sub>-GK-TCO-Tz-PEG<sub>4</sub>-Mal-5F7GGC ( $^{18}\text{F}$ -5F7GGC).

## MATERIALS AND METHODS

### sdAbs, Cells, Culture Conditions, and Animal Model

The anti-HER2 sdAb 5F7 and 5F7GGC, its analog with an engineered cysteine at the C terminus (19,20), were purchased from ATUM.

Cell culture reagents were purchased from Thermo Fisher Scientific and InvivoGen. HER2-expressing BT474 human breast carcinoma cells and its more metastatic version, BT474M1 (21), were cultured in RPMI 1640 medium containing 10% fetal bovine serum, 1% penicillin-streptomycin, 5  $\mu\text{g}/\text{mL}$  plasmosin, 1% sodium pyruvate, 1% 4-(2-hydroxyethyl)-1-piperazineethanesulfonic acid, and 0.4  $\mu\text{g}/\text{mL}$  insulin.

All procedures involving animals were approved by the Duke University institutional animal care and use committee. Female nude mice were obtained from an internal breeding colony at Duke or from Charles River Laboratories, and subcutaneous BT474M1 xenografts were established as previously described (7,11). Biodistribution and

imaging studies were initiated when tumors were 150–350  $\text{mm}^3$  in volume.

### Synthesis, Radiosynthesis, and $^{18}\text{F}$ Labeling of 5F7GGC

Details of the synthesis of the precursor (7), standard (8), and  $^{18}\text{F}$ -8, as well as the synthesis of *N*-succinimidyl 3-(guanidinomethyl)-5- $^{125}\text{I}$ -iodobenzoate (*iso*- $^{125}\text{I}$ -SGMIB), are provided in the supplemental materials (available at <http://jnm.snmjournals.org>). First, the sdAb was reduced to convert any dimer present to monomer. For this, a slurry of immobilized tris-[2-carboxyethyl] phosphine hydrochloride gel (Thermo Fisher Scientific; 300  $\mu\text{L}$ ) was added to a solution of 5F7GGC (1.5 mg, 115 nmol) in 300  $\mu\text{L}$  of 0.2 M  $\text{NH}_4\text{OAc}$  containing 5 mM ethylenediaminetetraacetic acid, pH 6.3, and the mixture was stirred at 37°C for 1 h. The suspension was centrifuged, and the supernatant containing monomeric 5F7GGC was immediately added to a vial containing methyltetrazine-PEG<sub>4</sub>-maleimide (0.18 mg, 345 nmol) and the mixture stirred at 37°C for 1 h. The Tz-5F7GGC product was isolated from the mixture by size-exclusion (SE) high-performance liquid chromatography (HPLC). For this, an Agilent PL Multisolvant 20 (7.8-mm internal diameter  $\times$  150 mm) SE-HPLC column was eluted in isocratic mode with water at a flow rate of 0.9 mL/min. The pooled HPLC fractions containing the Tz-5F7GGC ( $t_R = 3.3$  min) were lyophilized to obtain 0.5 mg of a pink solid. Its molecular weight was determined by liquid chromatography–mass spectrometry and binding affinity to HER2-Fc by surface plasmon resonance (supplemental materials). A solution of Tz-5F7GGC in phosphate-buffered saline, pH 7.4 (50  $\mu\text{L}$ , 2 mg/mL), was added to a vial containing dried  $^{18}\text{F}$ -8 (60–280 MBq), and the mixture was incubated at 37°C for 10 min.  $^{18}\text{F}$ -FN-PEG<sub>4</sub>-GK-TCO-Tz-PEG<sub>4</sub>-Mal-5F7GGC ( $^{18}\text{F}$ -5F7GGC) was isolated by gel filtration over a PD-10 column eluted with phosphate-buffered saline (20). Radiochemical purity, HER2 binding affinity, and immunoreactivity were determined as described previously (12), with details provided in the supplemental materials.

### Cellular Uptake and Internalization Assays

Paired-label uptake and internalization assays were performed on BT474M1 cells to compare the behavior of  $^{18}\text{F}$ -5F7GGC and *iso*- $^{125}\text{I}$ -SGMIB-5F7 sdAbs as described in the supplemental materials.

### Biodistribution Studies

The paired-label biodistribution of  $^{18}\text{F}$ -5F7GGC and *iso*- $^{125}\text{I}$ -SGMIB-5F7 was evaluated in athymic mice bearing subcutaneous BT474M1 xenografts. Groups of 5 mice received 166 kBq (0.64  $\mu\text{g}$ ) of *iso*- $^{125}\text{I}$ -SGMIB-5F7 and 666 kBq (3.6  $\mu\text{g}$ ) of  $^{18}\text{F}$ -5F7GGC in 100  $\mu\text{L}$  of phosphate-buffered saline via the tail vein. It was necessary to use a larger amount of activity and hence a larger mass for  $^{18}\text{F}$ -5F7GGC to compensate for the more rapid decay of  $^{18}\text{F}$ . Ex vivo biodistribution was determined at 1 and 3 h, and percentage injected dose (%ID)/g were calculated as previously described (7).

### Small-Animal PET/CT Imaging

Three BT474M1 tumor-bearing mice were imaged on a Siemens Inveon PET/CT system at 1, 2, and 3 h after injection of  $^{18}\text{F}$ -5F7GGC (1.6–2.2 MBq, 19–23  $\mu\text{g}$ ). The mice were anesthetized using 2%–3% isoflurane in oxygen, and a 5-min static PET acquisition followed by a 5-min CT scan was performed. List-mode PET data were histogram-processed, and the images were reconstructed using a standard algorithm consisting of 2 ordered-subsets-expectation-maximization

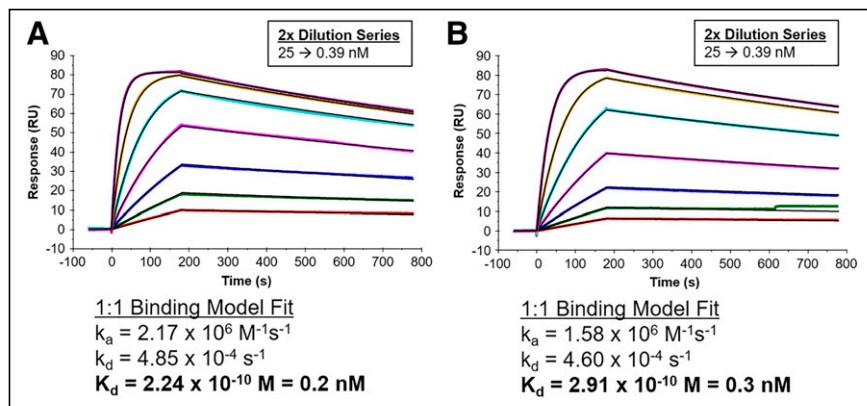


**FIGURE 2.** Sensorgrams showing dose–response curves and kinetic profiles for binding of 5F7 (A) and Tz-5F7GGC (B) to HER2-Fc extracellular domain.

3-dimensional iterations and 18 maximum-a-posteriori iterations with a cutoff (Nyquist) of 0.5. Images were corrected for attenuation (CT-based) and radioactive decay. Image analysis was performed using Inveon Research Workplace software.

### Statistical Analysis

Results are reported as mean  $\pm$  SD. The statistical significance of differences between coincubated or coadministered tracers was determined by a 2-tailed, paired Student *t* test (GraphPad QuickCalcs). A *P* value of less than 0.05 was considered to be significant.

## RESULTS

### Synthesis, sdAb Conjugation, and Radiochemistry

As shown in Supplemental Figure 1, the precursor **7** was synthesized from the known compound **1** (**22**) in 6 steps. Compound **8** was synthesized by treatment of **7** with tetra-*n*-butylammonium fluoride in 75.4% yield. The <sup>1</sup>H-nuclear magnetic resonance and mass spectrometry data for compounds **2–8** were consistent with their structures. Figure 1 shows the synthesis scheme for Tz-5F7GGC and its labeling via IEDDAR with <sup>18</sup>F-**8**. SE-HPLC–mass spectrometry analysis of the reaction mixture for 5F7GGC conjugation with methyltetrazine-PEG<sub>4</sub>-maleimide indicated complete conversion of 5F7GGC to Tz-5F7GGC (Supplemental Fig. 2). The observed molecular weight was consistent with its structure. Surface plasmon resonance indicated a *K<sub>d</sub>* of 0.3 nM (*k<sub>a</sub>* = 1.58  $\times$  10<sup>6</sup> M<sup>-1</sup>s<sup>-1</sup>; *k<sub>d</sub>* = 4.60  $\times$  10<sup>-4</sup> s<sup>-1</sup>) for Tz-5F7GGC versus 0.2 nM for 5F7, demonstrating that attaching the Tz-PEG<sub>4</sub>-Mal moiety had minimal effect on HER2 binding affinity (Fig. 2).

The radiochemical yield (RCY) for the synthesis of <sup>18</sup>F-FN-PEG<sub>4</sub>-GK-TCO (<sup>18</sup>F-**8**) from **7** via S<sub>N</sub>Ar reaction was 47.4%  $\pm$  9.0% (*n* = 11). With 100  $\mu$ g of protein at 2 mg/mL, the RCY for IEDDAR between Tz-5F7GGC and <sup>18</sup>F-**8** was 27.3%  $\pm$  8.2% (*n* = 4). Although performed only twice, use of 200  $\mu$ g of protein at 4 mg/mL increased conjugation yields to 46.1%  $\pm$  4.5%. Based on initial aqueous <sup>18</sup>F-fluoride activity, the total synthesis time for <sup>18</sup>F-5F7GGC was 90 min in an overall RCY of 8.9%  $\pm$  3.2% (*n* = 6) (7.3%  $\pm$  3.3% [*n* = 4] and 11.3%  $\pm$  0.4% [*n* = 2] for IEDDAR with 100  $\mu$ g and 200  $\mu$ g of sdAb, respectively). Although higher IEDDAR yields were obtained in the 200- $\mu$ g syntheses, RCYs for <sup>18</sup>F-**8** were low because of an HPLC malfunction. The molar activity for <sup>18</sup>F-5F7GGC was 5.2  $\pm$  2.7 MBq/nmol (*n* = 6). Sodium dodecyl sulfate polyacrylamide gel electrophoresis (Supplemental Fig. 3A) and SE-HPLC (Supplemental Fig. 3B) of <sup>18</sup>F-5F7GGC showed a single radioactive band/peak

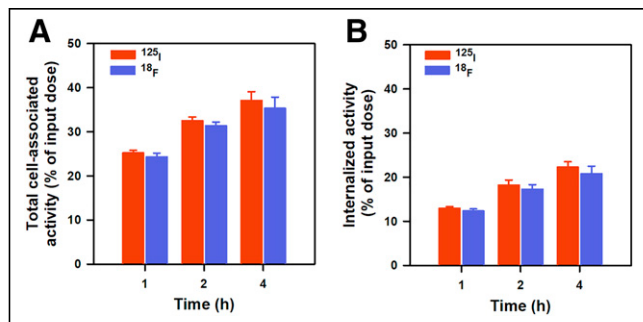


**FIGURE 3.** Paired-label uptake and internalization of *iso*-<sup>125</sup>I-SGMIB-5F7 and <sup>18</sup>F-5F7GGC by HER2-positive BT474M1 breast carcinoma cells. Data (mean  $\pm$  SD) are percentage of initially added activity that was bound to cells (membrane + internalized) (A) and internalized (B).

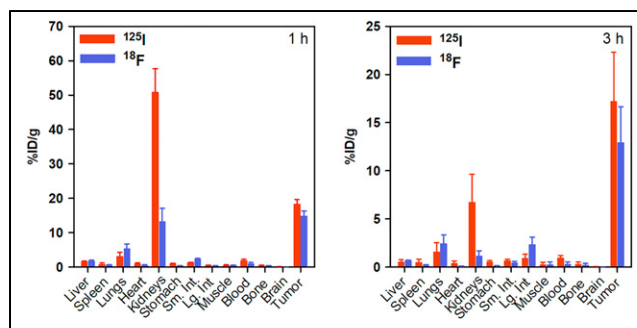


**FIGURE 4.** Paired-label biodistribution of <sup>18</sup>F-5F7GGC and *iso*-<sup>125</sup>I-SGMIB-5F7 sdAb conjugates in athymic mice bearing subcutaneous HER2-expressing BT474M1 breast carcinoma xenografts.

(~100%) corresponding to the molecular weight of an sdAb. The *K<sub>d</sub>* for binding of <sup>18</sup>F-5F7GGC to BT474 cells was 3.37  $\pm$  0.36 nM (Supplemental Fig. 3C) and its immunoreactive fraction 70.8% (Supplemental Fig. 3D), demonstrating that HER2 reactivity was not compromised with this <sup>18</sup>F-labeling strategy.

### Cell Uptake and Internalization Assay

After incubation with BT474M1 cells at 37°C, total cell-associated activity (Fig. 3A) for <sup>18</sup>F-5F7GGC was 24.3%  $\pm$  0.9%,

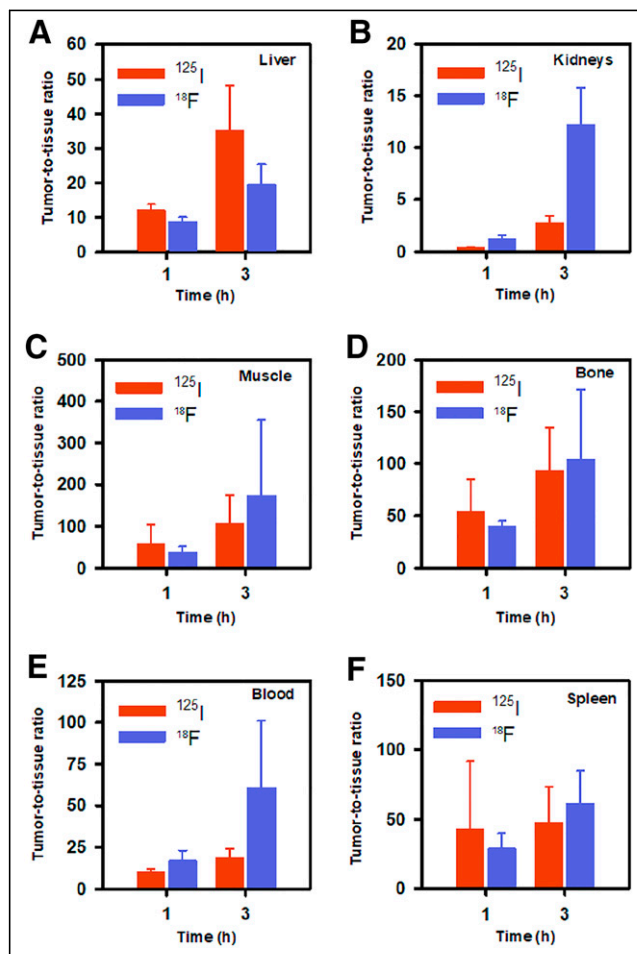


**FIGURE 5.** Tumor-to-tissue ratios after injection of <sup>18</sup>F-5F7GGC and *iso*-<sup>125</sup>I-SGMIB-5F7 sdAb conjugates in athymic mice bearing subcutaneous BT474M1 xenografts.

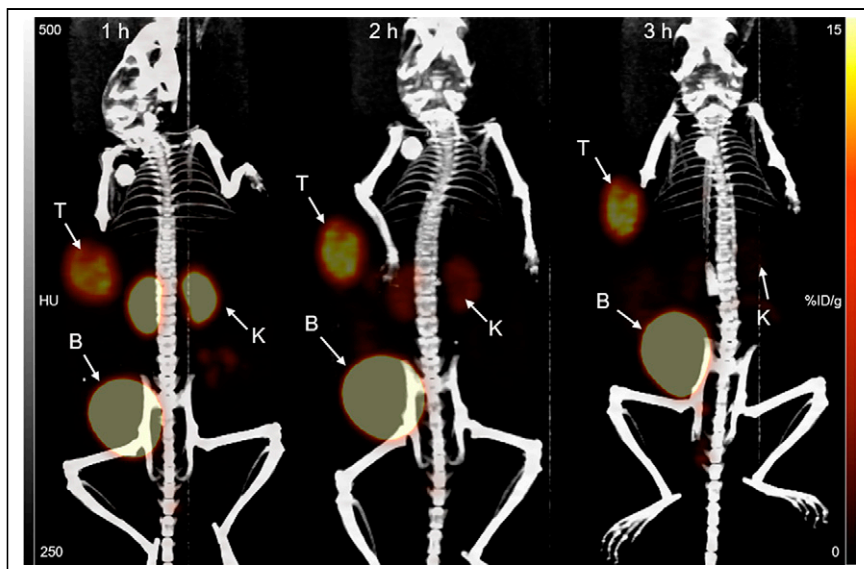


**FIGURE 6.** Maximum-intensity-projection  $^{18}\text{F}$ -5F7GGC immuno-PET images of representative mouse bearing subcutaneous HER2-positive BT474M1 xenograft obtained 1, 2, and 3 h after injection. Positions of tumor (T), kidney (K), and bladder (B) are indicated.

$31.3\% \pm 0.9\%$ , and  $35.3\% \pm 2.5\%$  of input activity at 1, 2, and 4 h, respectively, values that were slightly lower than those for coincubated *iso*- $^{125}\text{I}$ -SGMIB-5F7 ( $25.2\% \pm 0.6\%$ ,  $32.5\% \pm 0.8\%$ , and  $37.1\% \pm 2.0\%$ ); but differences between the radioconjugates were not statistically significant ( $P > 0.05$ ). Nonspecific uptake, determined at the 2-h time point by coincubation with excess trastuzumab, was less than 1% of input activity for both radiotracers. The percentage of input activity that was intracellularly trapped was  $12.3\% \pm 0.5\%$ ,  $17.3\% \pm 1.1\%$ , and  $20.8\% \pm 1.5\%$  for  $^{18}\text{F}$  and  $13.4\% \pm 4.4\%$ ,  $18.2\% \pm 1.2\%$ , and  $22.3\% \pm 1.2\%$  for  $^{125}\text{I}$  at 1, 2, and 4 h, respectively (Fig. 3B;  $P > 0.05$  for all).

#### Biodistribution

The data from the paired-label biodistribution of  $^{18}\text{F}$ -5F7GGC and *iso*- $^{125}\text{I}$ -SGMIB-5F7 in athymic mice bearing BT474M1 xenografts are presented in Figure 4. Tumor uptake of  $^{18}\text{F}$ -5F7GGC was similar to that seen for *iso*- $^{125}\text{I}$ -SGMIB-5F7 both at 1 h ( $^{125}\text{I}$ ,  $18.34 \pm 1.62\% \text{ID/g}$ ;  $^{18}\text{F}$ ,  $14.87 \pm 1.41\% \text{ID/g}$ ;  $P < 0.01$ ) and 3 h ( $^{125}\text{I}$ ,  $17.20 \pm 5.09\% \text{ID/g}$ ;  $^{18}\text{F}$ ,  $12.92 \pm 3.73\% \text{ID/g}$ ;  $P > 0.05$ ). On the other hand, with a few exceptions, normal-tissue activity for  $^{18}\text{F}$ -5F7GGC was similar to or less than that observed for *iso*- $^{125}\text{I}$ -SGMIB-5F7. Remarkably,  $^{18}\text{F}$ -activity levels in kidneys were 4- and 6-fold lower than those for  $^{125}\text{I}$  at 1 and 3 h, respectively. Bone uptake of  $^{18}\text{F}$  was low, suggesting limited susceptibility of  $^{18}\text{F}$ -5F7GGC to defluorination *in vivo*. Tumor-to-normal-tissue ratios for the 2 radiolabeled sdAbs are shown in Figure 5. Tumor-to-kidney ratios for  $^{18}\text{F}$  ( $1.2 \pm 0.4$  and  $12.2 \pm 3.5$ ) were 3.3- and 4.5-fold higher ( $P < 0.004$ ) than those for  $^{125}\text{I}$  ( $0.37 \pm 0.05$  and  $2.7 \pm 0.7$ ) at 1 and 3 h, respectively. Likewise, tumor-to-blood ratios were 2- to 3-fold higher for  $^{18}\text{F}$ . The tumor-to-liver ratio for  $^{18}\text{F}$ -5F7GGC was more than 5:1 at 1 h and lower than that for *iso*- $^{125}\text{I}$ -SGMIB-5F7 ( $P < 0.0003$ ).

#### Small-Animal PET/CT Imaging

Small-animal PET/CT maximum-intensity-projection images of a representative mouse bearing a subcutaneous BT474M1 xenograft

obtained 1, 2, and 3 h after administration of  $^{18}\text{F}$ -5F7GGC are shown in Figure 6. Consistent with the results from the necropsy study, pronounced tumor accumulation was observed at all time points, with minimal background activity except in kidneys and bladder. Kidney activity was quite low at 1 h, nearly undetectable by 2 h, and eliminated by 3 h, with bladder having prominent activity at all time points. The average tumor uptake values ( $n = 3$ ) calculated from the PET imaging data, expressed as  $\text{SUV}_{\text{max}}$  followed by  $\% \text{ID/g}_{\text{max}}$  in parentheses, were  $4.6 \pm 0.5$  ( $18.0 \pm 1.8$ ),  $4.7 \pm 0.9$  ( $17.9 \pm 3.6$ ), and  $5.0 \pm 0.8$  ( $19.0 \pm 3.1$ ) at 1, 2, and 3 h, respectively, with corresponding values for kidneys of  $2.9 \pm 0.3$  ( $11.2 \pm 1.0$ ),  $1.0 \pm 0.1$  ( $4.3 \pm 0.6$ ), and  $0.6 \pm 0.1$  ( $2.4 \pm 0.2$ ). Tumor-to-kidney ratios calculated from these PET imaging data were  $1.6 \pm 0.2$ ,  $4.2 \pm 0.6$ , and  $7.8 \pm 0.8$  at 1, 2, and 3 h, respectively.

#### DISCUSSION

Small protein platforms—exemplified herein by an sdAb—have favorable properties for immuno-PET including rapid tumor penetration and fast normal-tissue clearance and are ideally suited for use with  $^{18}\text{F}$ . However, because of their small size, they are much more likely than whole monoclonal antibodies to be adversely affected by chemical modification, resulting in unwanted normal-tissue retention or altered binding to their molecular target. Moreover, unlike monoclonal antibodies, retention of activity in the kidneys also can be problematic. To address these issues, we designed a labeling strategy (Fig. 1) comprising several synergistic components: a site-specific linker to control labeling location and stoichiometry (19), an RBBE-cleavable sequence to reduce kidney activity (12,14), a 6-fluoronicotinoyl group (13,14) to provide short-term residualization, and positioning the RBBE-cleavable sequence to avoid Tz- or TCO-bearing  $^{18}\text{F}$ -labeled catabolites *in vivo*.

Site-specific conjugation of the Tz-bearing maleimide with 5F7GGC was achieved without impairing HER2 binding of the sdAb (Fig. 2). The 48% RCY for TCO-bearing  $^{18}\text{F}$ -8 synthesis was reasonable given the presence of the free carboxyl group active hydrogens in compound 7, which is not generally conducive for labeling using nucleophilic  $^{18}\text{F}$ -fluoride (23). Of note,  $^{18}\text{F}$  labeling of TCO-bearing molecules was typically performed via the  $\text{S}_{\text{N}}2$  reaction, whereas in our case it was performed via the  $\text{S}_{\text{N}}\text{Ar}$  reaction, a first. RCYs for IEDDAR between Tz-5F7GGC and  $^{18}\text{F}$ -8 appeared to increase with increasing protein concentration but were lower than reported for  $^{18}\text{F}$  labeling using Tz-TCO IEDDAR in general (24) and for IEDDAR between TCO-modified sdAbs and  $^{18}\text{F}$ -labeled Tz derivatives in particular (12,14). A likely contributing factor is the number of prosthetic moieties per sdAb available for IEDDAR—when random conjugation was used, more than one TCO was attached per sdAb (12,14) versus just one Tz moiety in the current work. However, even with site-specific labeling, higher yields (53%–77%) have been reported for IEDDAR between  $^{18}\text{F}$ -TCO and a diabody site-

specifically modified with a Tz moiety (25). Differences in solvent, protein concentration, and polarity of the reagents between the 2 studies are noted, and these variables will be evaluated in future optimization of the current labeling strategy.

With the current procedure, the overall decay-corrected RCYs for the synthesis of  $^{18}\text{F}$ -5F7GGC were  $7.3\% \pm 3.3\%$  and  $11.3\% \pm 0.4\%$  at 100 and 200  $\mu\text{g}$  of Tz-5F7GGC, respectively, providing 154 and 237 MBq of  $^{18}\text{F}$ -5F7GGC from 3.7 GBq of aqueous  $^{18}\text{F}$ -fluoride in 90 min. On the basis of literature precedents (24), higher yields should be readily attainable by increasing protein levels beyond 200  $\mu\text{g}$ , which should be compatible with patient use given that a 1-mg sdAb dose was used in a phase 1 trial with another anti-HER2 sdAb labeled with  $^{68}\text{Ga}$  (26). That study used an average administered activity of 107 MBq of  $^{68}\text{Ga}$ , suggesting that with our current radiochemistry procedures, clinical studies would be feasible.

Multiple methods for labeling proteins with  $^{18}\text{F}$  have been reported (5). Random labeling of constituent protein lysine residues can be accomplished using active esters such as *N*-succinimidyl 4- $^{18}\text{F}$ -fluorobenzoate, 2,3,5,6-tetrafluorophenyl 6- $^{18}\text{F}$ -fluoronicotinate (13,27) and their 4-nitrophenyl analogs (28), among others. The site-specific  $^{18}\text{F}$  labeling of proteins also has been described, including via oxime formation with an engineered aminoxy function on the protein with 4- $^{18}\text{F}$ -fluorobenzaldehyde or preconjuncting the protein with maleimide-bearing agents containing moieties such as 4-fluorobenzaldehyde *O*-alkyl oxime, 4-SiFA, and AlF-chelate complex and subsequent  $^{18}\text{F}$  labeling of the conjugate (29,30). Of direct relevance to the current study, the last 3 approaches were evaluated for  $^{18}\text{F}$  labeling of an anti-HER2 Affibody. Although uptake in HER2-positive xenografts was reported, there were significant problems with each  $^{18}\text{F}$ -Affibody conjugate—either high uptake in the intestines or kidneys or excessive *in vivo* defluorination. From a radiochemistry perspective, it is important to note that the maleimide functionality is susceptible to  $\text{S}_{\text{N}}\text{Ar}$  and  $\text{S}_{\text{N}}2$   $^{18}\text{F}$ -labeling conditions and thus the maleimide-bearing part has to be conjugated to an  $^{18}\text{F}$ -bearing moiety, the synthesis of which often involves one or more steps. As mentioned above, an alternative approach of labeling proteins with  $^{18}\text{F}$  using maleimide agents involves conjugating them first with the maleimide-bearing agent and then performing the labeling under acidic pH and high temperatures (29); however, unfortunately, most proteins are not stable under these conditions. This led us to pursue the strategy described in the current work to exploit the very fast kinetics of IEDDAR under physiologic conditions. In addition, our strategy differs from those noted above in that it results in minimal background activity in the kidney and hepatobiliary organs as well as other tissues. Drawbacks of our method are the modest RCYs and relatively longer time for synthesis; however, systematic optimization of reaction conditions and other parameters should lead to a more efficient and streamlined procedure, which will be explored in future studies.

One of the main motivations for site-specific labeling is that it can provide a more homogeneous product and thereby facilitate clinical translation. In the conjugation of the prosthetic agent to the sdAb, a single product was obtained (Supplemental Fig. 2) whereas products with different levels (and likely sites) of substitution were observed with random lysine modification approaches (12,14). The other motivation is to avoid conjugation of the prosthetic agent on a lysine that could alter binding affinity. With 5F7 sdAb, this is a distinct possibility because 1 of its 5 lysines is located in CDR2 (20). However, a recent study showed no

difference in binding affinity for radioiodinated 5F7 conjugates prepared by site-specific and random labeling (19), suggesting either lack of modification or involvement in HER2 recognition for the CDR2 lysine. On the other hand, improvements in binding affinity have been demonstrated for site-specific modification of other sdAbs (31), making the affinity advantage possible through this labeling strategy dependent on the characteristics of the particular sdAb.

In previous work, *iso*-\*I-SGMIB emerged as the residualizing agent with the best combination of high tumor retention of radioactivity and low uptake in kidneys (9). Accordingly, *iso*- $^{125}\text{I}$ -SGMIB-5F7 was selected as the benchmark for use in these paired-label studies evaluating the HER2-targeting potential of  $^{18}\text{F}$ -5F7GGC. *In vitro* assays demonstrated HER2-specific uptake of  $^{18}\text{F}$ -5F7GGC on HER2-positive BT474M1 cells. Both total cell-associated and internalized activity for  $^{18}\text{F}$ -5F7GGC were not significantly different ( $P > 0.05$ ; Fig. 3) from those for coincubated *iso*- $^{125}\text{I}$ -SGMIB-5F7 and increased with time, demonstrating that the  $^{18}\text{F}$ -prosthetic agent is residualizing. Moreover, with the caveat that assay conditions were not the same, the cellular uptake and internalization of  $^{18}\text{F}$ -5F7GGC were similar to or higher than that seen previously with 5F7 labeled with  $^{18}\text{F}$  using other prosthetic agents (7,13,14).

Necropsy and small-animal PET imaging studies demonstrated rapid, high-level accumulation of  $^{18}\text{F}$ -5F7GGC in BT474M1 xenografts, suggesting that same-day immuno-PET imaging would be feasible. This is an important practical advantage compared with intact monoclonal antibodies such as  $^{89}\text{Zr}$ -trastuzumab that require up to 6 d to achieve optimal imaging conditions (32). Tumor uptake of  $^{18}\text{F}$ -5F7GGC was about 20%–25% lower than that of coinjected *iso*- $^{125}\text{I}$ -SGMIB-5F7, which might reflect the greater residualizing capacity of the guanidino versus the pyridyl moiety (33) or the presence of the GK linker (14). Nonetheless, with the caveat that different xenograft models were used,  $^{18}\text{F}$ -5F7GGC tumor uptake was higher than uptakes reported for most  $^{18}\text{F}$ -labeled anti-HER2 sdAb conjugates (8,12–14,34,35). A notable exception is the results obtained with  $^{18}\text{F}$ -RL-I-5F7 in the same BT474M1 xenograft (7); however, even though the less favorable SGMIB isomer (9) was used for 5F7 labeling, tumor uptake of radioiodine also was almost 2-fold that observed in the current study for *iso*- $^{125}\text{I}$ -SGMIB-5F7. Differences in mouse strain (NOD/SCID vs. athymic) between the 2 studies could play a role (36), as could individual xenograft properties such as tumor size (11), emphasizing the importance of performing experiments in paired-label format when possible.

Importantly, achieving high uptake in tumor with  $^{18}\text{F}$ -5F7GGC was not associated with increased uptake in the kidneys or other organs, which might hamper repeated use in patients to monitor HER2 status or interfere with lesion detection. This is an important distinction with agents such as  $^{18}\text{F}$ -RL-I-5F7, noted above, that show excellent tumor uptake but at the expense of sustained kidney activity levels higher than 100 %ID/g (7). Indeed, renal activity levels for  $^{18}\text{F}$ -5F7GGC were about 4–5 times lower than those for coadministered *iso*- $^{125}\text{I}$ -SGMIB-5F7, possibly the radio-labeled sdAb exhibiting the most rapid clearance of those investigated to date (1,9,37). It is likely that this behavior reflects both the presence of an RBBE-cleavable linker and the rapidly clearing 6- $^{18}\text{F}$ -fluoronicotinoyl moiety-containing catabolites (13). Finally, in our recent study evaluating 5F7 *iso*- $^{125}\text{I}$ -SGMIB conjugates formed by different linkers, use of the maleimido linker as done herein resulted in significantly decreased kidney uptake compared with the *N*-succinimidyl linker (19).

Compounds with both TCO and Tz moieties, especially Tz, are known to accumulate in hepatobiliary organs (38,39). For this reason, one of our design considerations was to strategically position the RBBE-cleavable linker in such a way that likely radiolabeled catabolites would be devoid of Tz and TCO moieties. We hypothesized that this would reduce uptake of activity levels in hepatobiliary organs, especially in intestines and gallbladder. Gratifyingly, uptake of activity from  $^{18}\text{F}$ -5F7GGC in the gut was more than 5 times lower than observed with a similar construct expected to generate radiolabeled catabolites bearing a Tz moiety (14). Consistent with this, whereas intense gallbladder uptake was observed in the small-animal PET images with the previous  $^{18}\text{F}$ -labeled sdAb conjugate (14), intestinal and gallbladder uptake was minimal or not observed for  $^{18}\text{F}$ -5F7GGC (Fig. 6). Importantly, the ratios for activity in tumor to liver and to bone, 2 frequent sites for HER2-positive tumor metastases, were 9:1 and 40:1, respectively, at 1 h after injection.

## CONCLUSION

A potentially widely applicable site-specific and residualizing  $^{18}\text{F}$ -labeling strategy for use with small proteins was validated using anti-HER2 sdAb 5F7. Strategic positioning of an RBBE-cleavable linker provided reduced activity levels in the kidneys and hepatobiliary organs. Moreover,  $^{18}\text{F}$ -5F7GGC demonstrated high potential as a probe for immuno-PET of HER2-expressing cancers.

## DISCLOSURE

This work was supported by National Institutes of Health grants CA188177 and CA42324. Michael R. Zalutsky holds ownership interest and is a board member for Cereius, Inc. Ganesan Vaidyanathan is a consultant and shareholder for Cereius, Inc. No other potential conflict of interest relevant to this article was reported.

## ACKNOWLEDGMENTS

We thank Dr. Xiao-Guang Zhao, Thomas Hawk, and Brian Watts for excellent technical assistance with the animal studies, small-animal PET/CT imaging, and surface plasmon resonance, respectively.

## KEY POINTS

**QUESTION:** Can a site-specific linker be devised for  $^{18}\text{F}$  labeling of small proteins that combines tumor-residualizing properties with rapid clearance of activity from kidneys and other normal tissues?

**PERTINENT FINDINGS:** An anti-HER2 sdAb with a C-terminal cysteine was site-specifically attached with a Tz derivative via maleimide-thiol conjugation and labeled with  $^{18}\text{F}$  by IEDDAR with a TCO agent attached to an  $^{18}\text{F}$ -fluoronicotinoyl moiety via a linker containing an RBBE-cleavable linker. The new  $^{18}\text{F}$ -sdAb conjugate exhibited high uptake in HER2-positive tumors with little activity in kidneys and other normal tissues on serial necropsy and small-animal PET imaging.

**IMPLICATIONS FOR PATIENT CARE:** This site-specific and residualizing  $^{18}\text{F}$ -labeling strategy could facilitate clinical translation of 5F7 anti-HER2 sdAb, as well as other sdAbs for immuno-PET.

## REFERENCES

1. Altunay B, Morgenroth A, Beheshti M, et al. HER2-directed antibodies, affibodies and nanobodies as drug-delivery vehicles in breast cancer with a specific focus on

- radioimmunotherapy and radioimmunoimaging. *Eur J Nucl Med Mol Imaging*. November 12, 2020 [Epub ahead of print].
2. Martin V, Cappuzzo F, Mazzucchelli L, Frattini M. HER2 in solid tumors: more than 10 years under the microscope—where are we now? *Future Oncol*. 2014;10:1469–1486.
3. Wolff AC, Hammond MEH, Allison KH, Harvey BE, McShane LM, Dowsett M. HER2 testing in breast cancer: American Society of Clinical Oncology/College of AMERICAN Pathologists clinical practice guideline focused update summary. *J Oncol Pract*. 2018;14:437–441.
4. Xavier C, Vaneycken I, D'Huyvetter M, et al. Synthesis, preclinical validation, dosimetry, and toxicity of  $^{68}\text{Ga}$ -NOTA-anti-HER2 nanobodies for iPET imaging of HER2 receptor expression in cancer. *J Nucl Med*. 2013;54:776–784.
5. Morris O, Fairclough M, Grigg J, Prenant C, McMahon A. A review of approaches to  $^{18}\text{F}$  radiolabelling affinity peptides and proteins. *J Labelled Comp Radiopharm*. 2019;62:4–23.
6. Vaidyanathan G, Zalutsky MR. Synthesis of *N*-succinimidyl 4- $^{18}\text{F}$ fluorobenzoate, an agent for labeling proteins and peptides with  $^{18}\text{F}$ . *Nat Protoc*. 2006;1:1655–1661.
7. Vaidyanathan G, McDougald D, Choi J, et al. Preclinical evaluation of  $^{18}\text{F}$ -labeled anti-HER2 nanobody conjugates for imaging HER2 receptor expression by immuno-PET. *J Nucl Med*. 2016;57:967–973.
8. Xavier C, Blykers A, Vaneycken I, et al.  $^{18}\text{F}$ -nanobody for PET imaging of HER2 overexpressing tumors. *Nucl Med Biol*. 2016;43:247–252.
9. Choi J, Vaidyanathan G, Koumariou E, Kang CM, Zalutsky MR. Astatine-211 labeled anti-HER2 5F7 single domain antibody fragment conjugates: radiolabeling and preliminary evaluation. *Nucl Med Biol*. 2018;56:10–20.
10. D'Huyvetter M, De Vos J, Xavier C, et al.  $^{131}\text{I}$ -labeled anti-HER2 camelid sdAb as a therapeutic tool in cancer treatment. *Clin Cancer Res*. 2017;23:6616–6628.
11. Pruszyński M, Koumariou E, Vaidyanathan G, et al. Improved tumor targeting of anti-HER2 nanobody through *N*-succinimidyl 4-guanidinomethyl-3-iodobenzoate radiolabeling. *J Nucl Med*. 2014;55:650–656.
12. Zhou Z, Devoogdt N, Zalutsky MR, Vaidyanathan G. An efficient method for labeling single domain antibody fragments with  $^{18}\text{F}$  using tetrazine-*trans*-cyclooctene ligation and a renal brush border enzyme-cleavable linker. *Bioconjug Chem*. 2018;29:4090–4103.
13. Zhou Z, McDougald D, Devoogdt N, Zalutsky MR, Vaidyanathan G. Labeling single domain antibody fragments with fluorine-18 using 2,3,5,6-tetrafluorophenyl 6- $^{18}\text{F}$ fluoronicotinate resulting in high tumor-to-kidney ratios. *Mol Pharm*. 2019;16:214–226.
14. Zhou Z, Zalutsky MR, Vaidyanathan G. Labeling a TCO-functionalized single domain antibody fragment with  $^{18}\text{F}$  via inverse electron demand Diels-Alder cycloaddition using a fluoronicotinyl moiety-bearing tetrazine derivative. *Bioorg Med Chem*. 2020;28:115634.
15. Chen Z, Chen M, Zhou K, Rao J. Pre-targeted imaging of protease activity through in situ assembly of nanoparticles. *Angew Chem Int Ed Engl*. 2020;59:7864–7870.
16. Gamache RF, Zettlitz KA, Tsai WTK, Collins J, Wu AM, Murphy JM. Tri-functional platform for construction of modular antibody fragments for in vivo  $^{18}\text{F}$ -PET or NIRF molecular imaging. *Chem Sci*. 2020;11:1832–1838.
17. Adumeau P, Sharma SK, Brent C, Zeglis BM. Site-specifically labeled immunconjugates for molecular imaging—part 1: cysteine residues and glycans. *Mol Imaging Biol*. 2016;18:1–17.
18. Fay R, Holland JP. The impact of emerging bioconjugation chemistries on radiopharmaceuticals. *J Nucl Med*. 2019;60:587–591.
19. Feng Y, Zhou Z, McDougald D, Meshaw RL, Vaidyanathan G, Zalutsky MR. Site-specific radioiodination of an anti-HER2 single domain antibody fragment with a residualizing prosthetic agent. *Nucl Med Biol*. 2021;92:171–183.
20. Pruszyński M, Koumariou E, Vaidyanathan G, et al. Targeting breast carcinoma with radioiodinated anti-HER2 nanobody. *Nucl Med Biol*. 2013;40:52–59.
21. Yu Z, Xia W, Wang HY, et al. Antitumor activity of an Ets protein, PEA3, in breast cancer cell lines MDA-MB-311DYT2 and BT474M1. *Mol Carcinog*. 2006;45:667–675.
22. Hamada T, Nishida A, Yonemitsu O. Selective removal of electron-accepting paratoluenesulfonyl and naphthalenesulfonyl protecting groups for amino function via photoinduced donor-acceptor ion-pairs with electron-donating aromatics. *J Am Chem Soc*. 1986;108:140–145.
23. Dornan MH, Simard JM, Leblond A, et al. Simplified and robust one-step radiosynthesis of [ $^{18}\text{F}$ ]DCFPyL via direct radiofluorination and cartridge-based purification. *J Labelled Comp Radiopharm*. 2018;61:757–763.
24. Otaru S, Imlimhan S, Sarparanta M, Helariutta K, Wahala K, Airaksinen AJ. Evaluation of organo [ $^{18}\text{F}$ ]fluorosilicon tetrazine as a prosthetic group for the synthesis of PET radiotracers. *Molecules*. 2020;25:1208.
25. Zettlitz KA, Waldmann CM, Tsai WK, et al. A dual-modality linker enables site-specific conjugation of antibody fragments for  $^{18}\text{F}$ -immuno-PET and fluorescence imaging. *J Nucl Med*. 2019;60:1467–1473.

26. Keyaerts M, Xavier C, Heemskerck J, et al. Phase I study of  $^{68}\text{Ga}$ -HER2-nanobody for PET/CT assessment of HER2 expression in breast carcinoma. *J Nucl Med.* 2016;57:27–33.
27. Olberg DE, Arukwe JM, Grace D, et al. One step radiosynthesis of 6- $^{18}\text{F}$ fluoronicotinic acid 2,3,5,6-tetrafluorophenyl ester ( $^{18}\text{F}$ -Py-TFP): a new prosthetic group for efficient labeling of biomolecules with fluorine-18. *J Med Chem.* 2010;53:1732–1740.
28. Haskali MB, Farnsworth AL, Roselt PD, Hutton CA. 4-Nitrophenyl activated esters are superior synthons for indirect radiofluorination of biomolecules. *RSC Med Chem.* 2020;11:919–922.
29. Glaser M, Iveson P, Hoppmann S, et al. Three methods for  $^{18}\text{F}$  labeling of the HER2-binding affibody molecule  $Z_{\text{HER2:2891}}$  including preclinical assessment. *J Nucl Med.* 2013;54:1981–1988.
30. Iveson PB, Glaser M, Indrevoll B, et al. FASTlab radiosynthesis of the  $^{18}\text{F}$ -labelled HER2-binding affibody molecule  $^{18}\text{F}$ GE-226. *J Labelled Comp Radiopharm.* 2019;62:925–932.
31. Kijanka M, Warmers F-J, El Khattabi M, et al. Rapid optical imaging of human breast tumor xenografts using anti-HER2 VHHs site-directly conjugated to IRDye 800CW for image-guided surgery. *Eur J Nucl Med Mol Imaging.* 2013;40:1718–1729.
32. Ulaner GA, Hyman DM, Ross DS, et al. Detection of HER2-positive metastases in patients with HER2-negative primary breast cancer using  $^{89}\text{Zr}$ -trastuzumab PET/CT. *J Nucl Med.* 2016;57:1523–1528.
33. Vaidyanathan G, Affleck DJ, Bigner DD, Zalutsky MR. Improved xenograft targeting of tumor-specific anti-epidermal growth factor receptor variant III antibody labeled using *N*-succinimidyl 4-guanidinomethyl-3-iodobenzoate. *Nucl Med Biol.* 2002;29:1–11.
34. Zhou Z, Chitneni SK, Devoogdt N, Zalutsky MR, Vaidyanathan G. Fluorine-18 labeling of an anti-HER2 VHH using a residualizing prosthetic group via a strain-promoted click reaction: chemistry and preliminary evaluation. *Bioorg Med Chem.* 2018;26:1939–1949.
35. Zhou Z, Vaidyanathan G, McDougald D, et al. Fluorine-18 labeling of the HER2-targeting single-domain antibody 2Rs15d using a residualizing label and preclinical evaluation. *Mol Imaging Biol.* 2017;19:867–877.
36. Lam K, Chan C, Reilly RM. Development and preclinical studies of  $^{64}\text{Cu}$ -NOTA-pertuzumab  $\text{F}(\text{ab}')_2$  for imaging changes in tumor HER2 expression associated with response to trastuzumab by PET/CT. *MAbs.* 2017;9:154–164.
37. Yang EY, Shah K. Nanobodies: next generation of cancer diagnostics and therapeutics. *Front Oncol.* 2020;10:1182.
38. García MF, Gallazzi F, Junqueira MS, et al. Synthesis of hydrophilic HYNIC-[1,2,4,5]tetrazine conjugates and their use in antibody pretargeting with  $^{99\text{m}}\text{Tc}$ . *Org Biomol Chem.* 2018;16:5275–5285.
39. Ruivo E, Adhikari K, Elvas F, et al. Improved stability of a novel fluorine-18 labeled TCO analogue for pretargeted PET imaging. *Nucl Med Biol.* 2019;76:77:36–42.